*Sensors and Materials*, Vol. 31, No. 4 (2019) 1241–1248
MYU Tokyo



S & M 1850

# Photoluminescence and Scintillation Properties of $Rb_2CeCl_5$ Crystal

Yutaka Fujimoto,[1*] Keiichiro Saeki,[1] Daisuke Nakauchi,[2] Takayuki Yanagida,[2] Masanori Koshimizu,[1] and Keisuke Asai[1]

[1]Department of Applied Chemistry, Graduate School of Engineering, Tohoku University, Sendai 980-8579, Japan
[2]Graduate School of Materials Science, Nara Institute of Science and Technology, 8916-5 Takayama, Ikoma, Nara 630-0192, Japan

(Received November 30, 2018; accepted March 25, 2019)

***Keywords:*** photoluminescence, scintillators, chloride, $Ce^{3+}$ 5d–4f transitions

A new $Rb_2CeCl_5$-based crystalline scintillator was grown by the vertical Bridgman–Stockbarger method for application in X-ray and gamma-ray detection. In the X-ray diffraction (XRD) analysis, most peaks of the grown crystal were in good agreement with the database of $Rb_2CeCl_5$, whereas a few peaks of $Rb_3CeCl_6$ were also identified. The photoluminescence and scintillation properties of a $Rb_2CeCl_5$ crystal were studied under excitation by UV light, X-rays, and γ-rays. The photoluminescence and scintillation spectra showed an emission band peak at 370 nm, with a shoulder at around 350 nm, which was assigned to the $5d^1$–4f ($^2F_{5/2}$, $^2F_{7/2}$) allowed transitions of $Ce^{3+}$. The calculated scintillation decay time constants were approximately 24 and 153 ns. The scintillation light yield reached 36000 photons/MeV with an energy resolution of 15% at 662 keV.

## 1. Introduction

An inorganic crystalline scintillator is a material that can efficiently absorb ionizing radiations and can convert a fraction of the incident radiation into a large number of low-energy photons in the ultraviolet (UV)–visible (VIS) range of the electromagnetic spectrum. Thus, the scintillator plays a central role in the detection and measurement of ionizing radiations such as X-rays and γ-rays. Some requirements for an ideal scintillator for X-rays and γ-rays include high light yield, high density ($\rho$), large effective atomic number ($Z_{eff}$), short decay time, excellent energy resolution, mechanical and chemical stability, and low cost. For the development of a radiation detector with good coincidence timing and high-count-rate capability, a scintillator with a combination of high light yield and short decay time is strongly required. Such a scintillator would be suitable for medical applications, particularly in time-of-flight positron emission tomography (TOF-PET).[(1–3)] Until the end of the 1990s, PET detectors were fabricated using $Bi_4Ge_3O_{12}$ (BGO) single crystals, which were optically coupled to photomultiplier tubes (PMTs). Since its discovery in 1990, the $Lu_2SiO_5$:Ce single crystal has been extensively studied

*Corresponding author: e-mail: fuji-you@qpc.che.tohoku.ac.jp
https://doi.org/10.18494/SAM.2019.2183

ISSN 0914-4935 
https://myukk.org/

and has become the candidate of choice for replacing BGO in a TOF-PET detector because of its short decay time (~40 ns) and high light yield (~27000 photons/MeV). Despite this discovery, there is room for the improvement of existing scintillators, and the development of new fast scintillators to further advance the timing resolution of the TOF-PET is desired.

Various fast crystalline scintillators fabricated using oxides, fluorides, and other halide crystals have been reported. Although barium fluoride ($BaF_2$) has been reported to have the shortest decay time (~0.7 ns), the emission band owing to core-valence luminescence (CVL) is located at wavelengths between 190 and 220 nm;[4] hence, $BaF_2$ scintillators require a UV-enhanced PMT and a photodiode (PD). We also studied some CVL scintillators showing UV–VIS emission bands for chloride-based crystals. In particular, $Cs_2ZnCl_4$ and $CsCaCl_3$ have fast CVL bands (~1.8 ns for $Cs_2ZnCl_4$ and ~2.3 ns for $CsCaCl_3$) in the VIS wavelength range, but their light yield is poor for pulse-counting measurements.[5–6] Other fast scintillators include $Yb^{3+}$-,[7] $Pr^{3+}$-,[8] $Nd^{3+}$-,[9] and $Ce^{3+}$-doped[10–12] single crystals, and transparent polycrystalline ceramics for γ-ray spectroscopy.

Currently, we focus on cerium-based self-activated halide scintillators such as $CsCe_2Cl_7$,[13] $Cs_3CeCl_6$,[13] $K_2CeCl_5$,[14–15] $K_2CeBr_5$,[16] $Cs_2NaCeCl_6$,[17] $Cs_2NaCeBr_6$,[18] $Cs_2LiCeCl_6$,[19] $Cs_2LiCeBr_6$,[20] and $Rb_2LiCeBr_6$,[21] and scintillators for next-generation TOF-PET detectors because of the large atomic number of Ce ($Z$ = 58), as well as their high light yields and short decay times due to the 5d-4f allowed transitions of $Ce^{3+}$. Moreover, unlike other halide scintillators, cerium-based scintillators do not require dopant elements as emission centers, resulting in a decrease in production cost. In particular, the $MX$-$CeX_3$ ($M$ = alkali metal, $X$ = Cl, Br, or I)-based ternary halide crystals show good chemical and scintillating performance, including a high light yield with a short decay time and a low hygroscopicity. Thus, in this study, we investigated a new cerium-based self-activated halide scintillator of $Rb_2CeCl_5$ that has moderate $\rho$ (= 3.36 g/cm$^3$) and large $Z_{eff}$ (= 44.5), grown using the vertical Bridgman–Stockbarger method because the crystal is expected to show the same type of fast and bright scintillation due to $Ce^{3+}$. To the best of our knowledge, no other study on the photoluminescence and scintillation properties of crystalline $Rb_2CeCl_5$ has been reported so far.

## 2. Experimental Procedure

$Rb_2CeCl_5$ crystals were grown in vacuum using the vertical Bridgman–Stockbarger method. Quartz ampoules to be used for crystal growth were cleaned in a strong alkali solution (sodium hydroxide) to remove organic impurities, such as grit and dust, and then thoroughly rinsed with ultrapure water. Then, the ampoules were annealed at 1000 °C in an electric furnace for 24 h for the removal of water into ampoules. Stoichiometric amounts of RbCl (4N) and $CeCl_3{\cdot}7H_2O$ (3N) starting materials were loaded into the clean quartz ampoules. The materials were subsequently dried in vacuum at 623 K for 24 h to remove the fluid. The ampoule was sealed under high vacuum, and the $Rb_2CeCl_5$ crystals were grown in two zone furnaces at a temperature gradient of 1.3 °C/mm using the Bridgman method. The temperatures of the upper and lower zones in the vertical furnace were 973 and 773 °C, respectively. The crystal synthesis was carried out at a growth rate between 1.0 and 3.0 mm/h. The powder X-ray diffraction (XRD) analysis of

part of an as-grown crystal was performed in the $2\theta$ range from 5 to 80° using an Ultima IV diffractometer (RIGAKU).

The excitation and emission spectra were recorded using a Hitachi F-7000 fluorescence spectrophotometer equipped with a xenon lamp as the excitation source. The fluorescence quantum efficiency (QE) was evaluated using a Quantaurus-QY (Hamamatsu Photonics) spectrofluorometer equipped with a xenon lamp and a calibrated integrating sphere.

The photoluminescence decay was measured using a DeltaFlex time-correlated single photon counting (TCSPC; Horiba) device equipped with a light-emitting diode (LED) as the excitation source. The specimen was excited at 325 nm using a pulsed NanoLED excitation source, and the photoluminescence photons from the specimen were counted using a picosecond photon detection (PPD)-850 module. To determine the decay time constant, the obtained decay curves were fitted with appropriate multiexponential decay functions.

The scintillation spectrum was obtained through X-ray excitation from an X-ray generator (RINT2200, Rigaku) equipped with a copper target at power settings of 40 kV and 40 mA. The scintillation photons from the specimen were counted with a SILVER-Nova multichannel spectrometer (Stellarnet Inc.), which was cooled to −15 °C by a Peltier module through an optical fiber. The crystal specimen was optically coupled to the fiber head using optical grease, with Teflon tape as a reflector to increase the light collection of diffuse reflections.

The scintillation-decay time profile, obtained under excitation with pulsed X-rays, was measured using our original setup with a pulsed X-ray-induced afterglow characterization system (Hamamatsu Photonics).[22] This enabled the observation of scintillation characteristics in the wavelength range between 160 and 650 nm with a time resolution of 1.0 ns.

The $^{137}$Cs-γ-ray-induced scintillation pulse height spectrum was measured by optically coupling the specimen to a R7600U-200 (Hamamatsu Photonics) PMT. A detailed explanation for the setup can be found in our previous report.[7] The bias voltage of PMT during the measurement was set to 600 V, and the spectrum of the $Rb_2CeCl_5$ crystal was recorded with a shaping time of 0.5 μs. The scintillation light yield was calculated by comparing the 662 kV γ-ray photopeak channel in the spectrum with that of a NaI:Tl commercial scintillator (LY = ~40000 photons/MeV, $\lambda_{em}$ = 415 nm, shaping time: 2 μs) using similar experimental conditions.

## 3. Results and Discussion

### 3.1 Grown crystal sample and XRD analysis

A grown crystal specimen of $Rb_2CeCl_5$ is shown in Fig. 1(a), and the analyzed powder XRD patterns are shown in Fig. 1(b). Most peaks of the grown crystal were in good agreement with the Springer Materials online database, $Rb_2CeCl_5$ (sd_1705854), whereas a few peaks of $Rb_3CeCl_6$ were also identified, indicating that the grown crystal contained a slight $Rb_3CeCl_6$ crystalline phase (ICSD No. 00-038-1318). The contamination of the secondary phase that may act as electron (or hole)-trapping centers has a large effect on the scintillation process. The crystal specimen was subsequently sliced and polished for use in photoluminescence and scintillation measurements. Visual observation indicated that the crystal is less hygroscopic

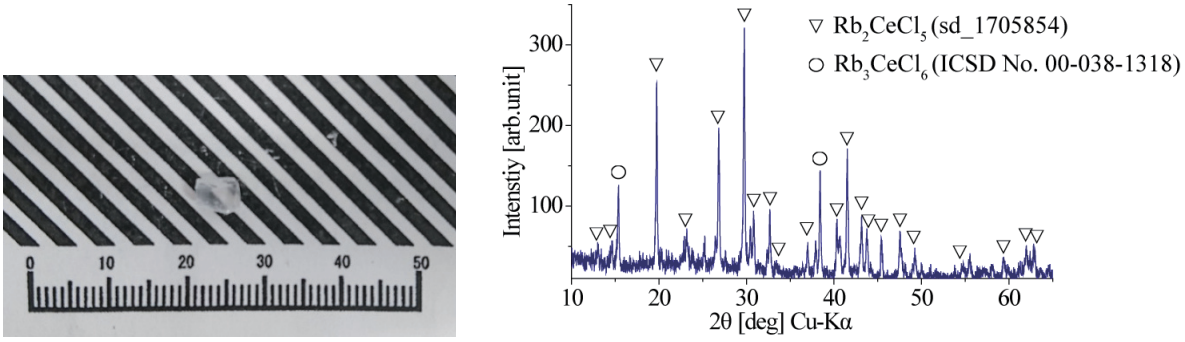


(a) (b)

Fig. 1. (Color online) Photograph of (a) an as-grown crystal and (b) X-ray diffraction patterns of $Rb_2CeCl_5$.

than $LaBr_3$:Ce and $SrI_2$:Eu crystals; hence, we performed the photoluminescence and scintillation measurements in air.

### 3.2 Excitation and emission spectra and photoluminescence decay curves

The obtained excitation and emission spectra are shown in Fig. 2. The excitation spectrum, monitored at an emission wavelength of 370 nm, showed at least five excitation bands in the wavelength range from 200 to 330 nm. These excitation bands corresponded to the transitions from 4f ground states to $5d^5$ (~210 nm), $5d^4$ (~237nm), $5d^3$ (~255 nm), $5d^2$ (~300 nm), and $5d^1$ (~325 nm) excited states of $Ce^{3+}$. Upon UV excitation at 325 nm, the characteristic $Ce^{3+}$ $5d^1$–4f ($^2F_{5/2}$, $^2F_{7/2}$) emission band was observed at 370 nm with a shoulder at around 350 nm. A similar emission band was reported previously for crystalline $K_2CeCl_5$ and $CsCe_2Cl_6$.[13,14] The Stokes shift of the $Ce^{3+}$ emission for $Rb_2CeCl_5$ was calculated to be about 3,742 $cm^{-1}$ (~0.46 eV). Such a small Stokes shift, combined with a large crystal field splitting, has been reported for other Ce-based self-activated halide scintillators.[13,23] The shoulder band could be attributed to self-absorption caused by spectral overlap between the excitation and emission bands, which was observed previously for crystalline $K_2CeCl_5$ and $CsCe_2Cl_6$.[13,14] The fluorescence QE for the $Ce^{3+}$ $5d^1$–4f emissions was calculated to be approximately 60% under excitation by 325 nm light.

Figure 3 shows the photoluminescence decay curves obtained at emission bands of 350 (pink line) and 370 (blue line) nm. The calculated decay time constants at 350 nm emission were approximately 4 and 27 ns; the corresponding decay constants at 370 nm were approximately 7 and 41 ns. The fast decay time components of 4 and 7 ns are due to an instrumental response function that is typically measured as a response of the instrument to scattered excitation pulse. The shorter decay time constant at 350 nm may be caused by the quenching of the $Ce^{3+}$ emission due to the self-absorption effect because of the small Stokes shift.

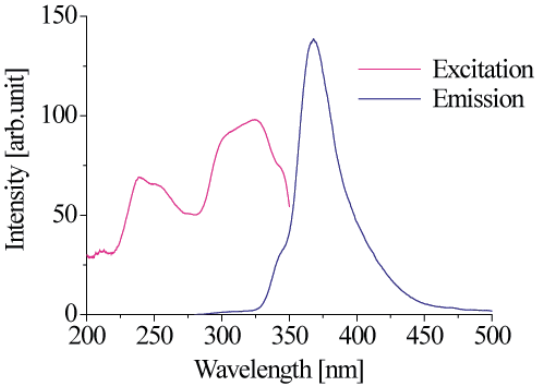


Fig. 2. (Color online) Excitation (pink line) and emission (blue line) spectra of crystalline $Rb_2CeCl_5$.

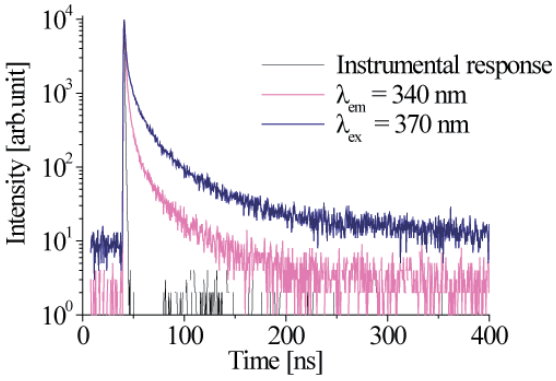


Fig. 3. (Color online) Photoluminescence decay curves of crystalline $Rb_2CeCl_5$, monitored at emission bands of 350 (pink line) and 370 (blue line) nm.

### 3.3 Scintillation spectrum and decay time profile

The scintillation spectrum obtained under X-ray excitation is provided in Fig. 4. The spectrum shows two emission bands in the UV region peaked at 370 and 350 nm, which is consistent with the photoluminescence, and can thus be assigned to the transitions from the $5d^1$ excited state to the 4f ($^2F_{5/2}$, $^2F_{7/2}$) ground states owing to $Ce^{3+}$. No other emission band is observed in the spectrum, which excludes the possibility of self-trapped excitons (STEs), CVL, lattice defects, and impurities. The emission wavelength of the $Ce^{3+}$ matches well with the spectral sensitivity of conventional PMTs.

Figure 5 shows the pulsed X-ray-induced scintillation decay time profile. In the measurements, scintillation photons in the wavelength range from 160 to 650 nm were counted using the PMT. The decay time constants were calculated to be approximately 8 (44%), 24 (54%), and 153 (1%) ns. The fast decay time components of 8 ns were due to an instrumental response function, whereas the other components were due to the $Ce^{3+}$ emission. From the calculation, the short decay time constant of 24 ns was found to be the major component. The short component with a decay time constant of 24 ns is at the typical level for $Ce^{3+}$ emission, whereas the decay time constant is smaller than that of the photoluminescence one (~41 ns). The mechanism of the difference in decay time between photoluminescence and scintillation has not yet been clarified; however, we speculate that it is due to a complex energy transfer process from the host crystal lattice to emission centers and quenching under excitation by ionizing radiation. The primary decay time constants of some cerium-based self-activated halide scintillators previously reported were 50 ns for $CsCe_2Cl_7$ and $Cs_3CeCl_6$,[13] 78 ns for $K_2CeCl_5$,[15] 91 ns for $Cs_2NaCeCl_6$,[17] 140 ns for $Cs_2NaCeBr_6$,[18] 101 ns for $Cs_2LiCeCl_6$,[19] 86 ns for $Cs_2LiCeBr_6$,[20] and 55 ns for $Rb_2LiCeBr_6$.[21] Therefore, the scintillation of $Rb_2CeCl_5$ compared with those scintillators is relatively fast.

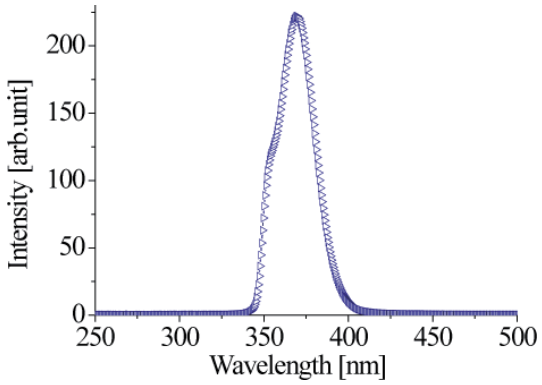


Fig. 4. (Color online) X-ray-induced scintillation spectrum of crystalline $Rb_2CeCl_5$.

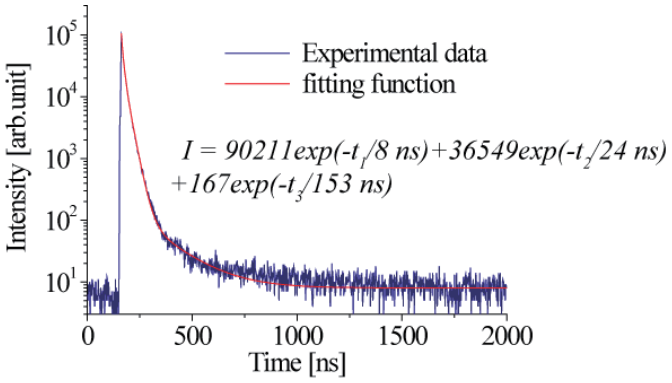


Fig. 5. (Color online) Decay time profile of pulsed X-ray-excited scintillation for crystalline $Rb_2CeCl_5$.

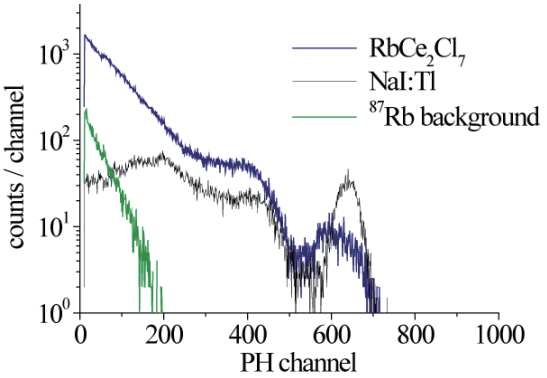


Fig. 6. (Color online) Scintillation pulse height spectrum of crystalline $Rb_2CeCl_5$ (blue line) compared with that of a NaI:Tl scintillator (black line).

### 3.4 Scintillation pulse height spectrum

The scintillation pulse height spectrum obtained under excitation by $^{137}$Cs γ-rays is shown in Fig. 6. The spectrum of the NaI:Tl commercial scintillator (black line) is presented for comparison of the scintillation light yields. Because of the $^{87}$Rb radioactive isotope within the crystal, a background spectrum (green line) was also recorded without a sealed $^{137}$Cs γ-ray source under the same conditions as those for the $^{137}$Cs-induced pulse height spectra. The $^{87}$Rb isotope (with a natural abundance of 28%) emits $\beta$-particles with an end-point energy of 283 keV.[21,24] To determine the photopeak channel and energy resolution, each photopeak was fitted using a Gaussian curve. In the spectra, the $^{137}$Cs-662 keV gamma-ray photopeak for $Rb_2CeCl_5$ is located at 602 channels, whereas that of NaI:Tl is observed at 638 channels. The QEs of the R7600U PMT at 370 nm ($Rb_2CeCl_5$) and 415 nm (NaI:Tl) were about 42 and 40%, respectively. Thus, the light yield for $Rb_2CeCl_5$ was estimated to be approximately 36000 photons/MeV by comparison with the data for NaI:Tl. The energy resolution of $Rb_2CeCl_5$ and NaI:Tl was estimated from the full width at half maximum (FWHM) of the 662 keV γ-ray photopeak. The

energy resolution for $Rb_2CeCl_5$ was calculated to be approximately 15%, whereas that of NaI:Tl was 7.3%. From these results, $Rb_2CeCl_5$ was found to show a poor energy resolution despite the high light yield. This may originate from the low crystalline quality and existence of the secondary phase in the crystal sample grown in this study.

## 4. Summary

We present the results of an initial study of a $Rb_2CeCl_5$ crystalline scintillator, which was grown using the vertical Bridgman–Stockbarger method. The XRD patterns indicated that the grown crystal contained a slight $Rb_3CeCl_6$ crystalline phase. Under excitation by UV light and X-rays, the scintillation spectrum showed the characteristic $Ce^{3+}$ $5d^1$–4f ($^2F_{5/2}$, $^2F_{7/2}$) emission band at 370 nm with a shoulder at around 350 nm. The scintillation decay time constants corresponded to two components, which were approximately 24 and 153 ns. The scintillation light yield was estimated to be approximately 36000 photons/MeV by comparison with the data for a NaI:Tl commercial scintillator. The good scintillation light yield performance, combined with the short decay time, indicated that the $Rb_2CeCl_5$ crystalline scintillator could be a promising candidate for X-ray and γ-ray detector applications, having good coincidence timing and high-count-rate capability. The drawbacks of these scintillators are their poor energy resolution and the presence of the $^{87}Rb$ isotope (27.8% in natural abundance) in the crystal, which produces an intrinsic radiation background in the low-energy regions during the pulse-counting measurements.

## Acknowledgments

This work was partially supported by the Cooperative Research Project of the Research Institute of Electronics, Shizuoka University.

## References

1 C. L. Melcher: J. Nucl. Med. **41** (2000) 1051.
2 C. W. E. Van Eijk: Radiat. Prot. Dosim. **129** (2008) 13.
3 P. Lecoq: Nucl. Instrum. Methods Phys. Res., Sect. A **809** (2016) 130.
4 T. Yanagida, Y. Fujimoto, A. Yoshikawa, Y. Yokota, K. Kamada, J. Pejchal, N. Kawaguchi, K. Fukuda, K. Uchiyama, K. Mori, K. Kitano, and M. Nikl: Appl. Phys. Exp. **3** (2010) 056202.
5 N. Yahaba, M. Koshimizu, Y. Sun, T. Yanagida, Y. Fujimoto, R. Haruki, F. Nishikido, S. Kishimoto, and K. Asai: Appl. Phys. Exp. **7** (2014) 062602.
6 M. Koshimizu, N. Yahaba, R. Haruki, F. Nishikido, S. Kishimoto, and K. Asai: Opt. Mater. **36** (2014) 1930.
7 T. Yanagida, Y. Fujimoto, H. Yagi, and T. Yanagitani: Opt. Mater. **36** (2014) 1044.
8 T. Yanagida, Y. Fujimoto, K. Kamada, D. Totsuka, H. Yagi, T. Yanagitani, Y. Futami, S. Yanagida, S. Kurosawa, Y. Yokota, A. Yoshikawa, and M. Nikl: IEEE Trans. Nucl. Sci. **59** (2012) 2146.
9 T. Yanagida, K. Fukuda, N. Kawaguchi, S. Kurosawa, Y. Fujimoto, Y. Futami, Y. Yokota, K. Taniue, H. Sekiya, H. Kubo, A. Yoshikawa, and T. Tanimori: Nucl. Instrum. Methods Phys. Res., Sect. A **659** (2011) 258.
10 V. G. Baryshevsky, M. V. Korzhik, V. I. Moroz, V. B. Pavlenko, A. A. Fyodorov, S. A. Smirnova, O. A. Egorycheva, and V. A. Kachanov: Nucl. Instrum. Methods Phys. Res., Sect. B **58** (1991) 291.
11 C. L. Melcher and J. S. Schweitzer: IEEE Trans. Nucl. Sci. **39** (1992) 502.
12 E. V. D. van Loef, P. Dorenbos, C. W. E. van Eijk, K. W. Kramer, and H. U. Gudel: Nucl. Instrum. Methods Phys. Res., Sect. A **486** (2002) 254.

13 M. Zhuravleva, K. Yang, and C. L. Melcher: J. Cryst. Growth **318** (2011) 809.
14 U. N. Roy, M. Groza, Y. Cui, A. Burger, N. Cherepy, S. Friedrich, and S. A. Payne: Nucl. Instrum. Methods Phys. Res., Sect. A **579** (2007) 46.
15 E. Rowe, E. Tupitsyn, P. Bhattacharya, L. Matei, M. Groza, V. Buliga, G. Atkinson, and A. Burger: J. Cryst. Growth **393** (2014) 156.
16 R. Hawrami, A. K Batra, M. D Aggarwal, U. N. Roy, M. Groza, Y. Cui, A. Burger, N. Cherepy, T. Niedermayr, and S. A. Paynec: J. Cryst. Growth **310** (2008) 2099.
17 G. Rooh, H. Kang, H. J. Kim, H. Park, and S. Kim: J. Cryst. Growth **311** (2009) 2470.
18 S. Kim, G. Rooh, H. J. Kim, W. Kim, and U. Hong: IEEE Trans. Nucl. Sci. **57** (2010) 1251.
19 G. Rooh, H. J. Kim, and S. Kim: IEEE Trans. Nucl. Sci. **57** (2010) 1255.
20 J. K. Cheon, S. Kim. G. Rooh, J. H. So, H. J. Kim, and H. Park: Nucl. Instrum. Methods Phys. Res., Sect. A **652** (2011) 205.
21 G. Rooh, H. Kim, H. Park, and S. Kim: IEEE Trans. Nucl. Sci. **57** (2010) 3836.
22 T. Yanagida, Y. Fujimoto, T. Ito, K. Uchiyama, and K. Mori: Appl. Phys. Exp. **7** (2014) 062401.
23 C. Pedrini, A. N. Belsky, B. Moine, and D. Bouttet: Acta Phys. Pol. A **84** (1993) 953.
24 C. W. E. Van Eijk, J. T. M. de Haas, P. Dorenbos, K. W. Krämer, and H. U. Güdel: IEEE Nucl. Sci. Symp. Conf. Rec. **3** (2005) 239.